Provided for non-commercial research and education use.
Not for reproduction, distribution or commercial use.

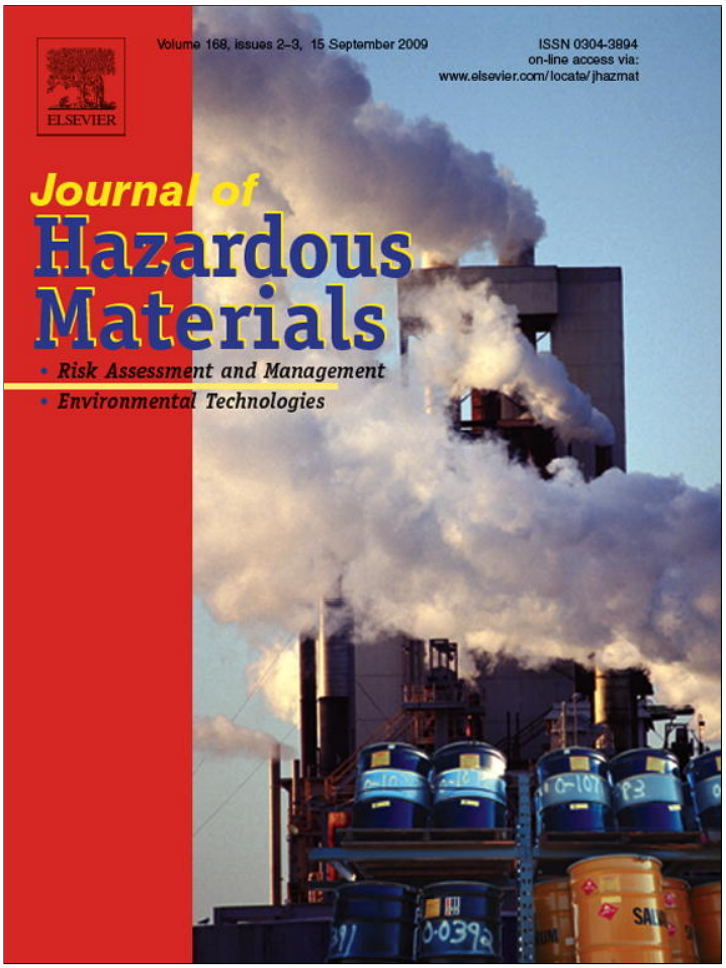

This article appeared in a journal published by Elsevier. The attached copy is furnished to the author for internal non-commercial research and education use, including for instruction at the authors institution and sharing with colleagues.

Other uses, including reproduction and distribution, or selling or licensing copies, or posting to personal, institutional or third party websites are prohibited.

In most cases authors are permitted to post their version of the article (e.g. in Word or Tex form) to their personal website or institutional repository. Authors requiring further information regarding Elsevier's archiving and manuscript policies are encouraged to visit:

http://www.elsevier.com/copyright

Author's personal copy

Journal of Hazardous Materials 168 (2009) 711–720

Contents lists available at ScienceDirect

Journal of Hazardous Materials

journal homepage: www.elsevier.com/locate/jhazmat

Material and structural characterization of alkali activated low-calcium brown coal fly ash

František Škvára[a,*], Lubomír Kopecký[b,1], Vít Šmilauer[b,1], Zdeněk Bittnar[b,1]

[a] ICT Prague, Faculty of Chemical Engineering, Department of Glass and Ceramics, 166 28 Prague 6, Technická 5, Czech Republic
[b] Czech Technical University in Prague, Faculty of Civil Engineering, Department of Mechanics, 166 29 Prague 6, Thákurova 7, Czech Republic

ARTICLE INFO

Article history:
Received 5 July 2008
Received in revised form 5 December 2008
Accepted 17 February 2009
Available online 25 February 2009

Keywords:
Inorganic polymer
Geopolymer
Alkali activation
Fly ash
Microstructure
Heavy metal immobilization

ABSTRACT

The waste low-calcium Czech brown coal fly ash represents a considerable environmental burden due to the quantities produced and the potentially high content of leachable heavy metals. The heterogeneous microstucture of the geopolymer M_n $[-(Si-O)_z-Al-O]_n \cdot wH_2O$, that forms during the alkaline activation, was examined by means of microcalorimetry, XRD, TGA, DSC, MIP, FTIR, NMR MAS (^{29}Si, ^{27}Al, ^{23}Na), ESEM, EDS, and EBSD. The leaching of heavy metals and the evolution of compressive strength were also monitored. The analysis of raw fly ash identified a number of different morphologies, unequal distribution of elements, Fe-rich rim, high internal porosity, and minor crystalline phases of mullite and quartz. Microcalorimetry revealed exothermic reactions with dependence on the activator alkalinity. The activation energy of the geopolymerization process was determined as 86.2 kJ/mol. The X-ray diffraction analysis revealed no additional crystalline phases associated with geopolymer formation. Over several weeks, the ^{29}Si NMR spectrum testified a high degree of polymerization and Al penetration into the SiO_4 tetrahedra. The ^{23}Na NMR MAS spectrum hypothesized that sodium is bound in the form of $Na(H_2O)_n$ rather than Na^+, thus causing efflorescence in a moisture-gradient environment. As and Cr^{6+} are weakly bonded in the geopolymer matrix, while excellent immobilization of Zn^{2+}, Cu^{2+}, Cd^{2+}, and Cr^{3+} are reported.

Crown Copyright © 2009 Published by Elsevier B.V. All rights reserved.

1. Introduction

Over 55% of the total electric power produced in the Czech Republic originates from domestic brown coal power plants. Considerable quantities of inorganic waste materials (fly ash, gypsum) arise as an undesirable by-product. The amount of fly ash annually exceeds one tone per capita in the Czech Republic while only a small part is blended with Portland cement or used as a stabilizing material in soil beds. Unfortunately, the majority of fly ash is deposited into mined-out open pits where it is usually mixed with waste gypsum arising from the smoke desulphurization within power plants.

When compared with other locations in Europe, Czech brown fly ash differs in composition as well as in content of toxic elements plus heavy metals such as As. The differences are caused by the geological evolution of the Northern Bohemian brown coal basin during the Tertiary era, where the weathering of rocks rich in metals ores created a substantial part of sediments for the coal basin. The disposal of fly ash is one of the most pressing ecological problems and the idea of reutilization certainly deserves attention. One promising method appears to produce a new construction material, a geopolymer, emerging through the process of alkali activation of raw fly ash (RFA).

As shown by Purdon in 1940 [1], water-soluble alkali compounds accelerate the hydration process of hydraulic and latently hydraulic materials (slags) and enable the evolution of new hydraulic phases. In 1959, Gluchovskij described in his book "Gruntosilikaty" [2], the possibilities of the preparation of new construction materials by the reaction of alumino-silicate materials with alkali compounds (carbonates, hydroxides, silicates). During the years 1976–1979, Davidovits [3] coined the term *geopolymer*. According to his statement, geopolymers are materials that originate by inorganic poly-condensation, called geopolymeration.

Geopolymer materials are based on two to three dimensional structure of the M_n $[-(Si-O)_z-Al-O]_n \cdot wH_2O$ type where M stands for alkaline cation Na^+ or K^+. The geopolymers represent materials on the transition between glass and ceramics and materials based on standardized inorganic binders. The geopolymers may be used as inorganic binders in the construction materials produced from the alumino-silicate wastes, as has been presented at numerous conferences (Kiew 1978, 1985, 1989, 1994, 1999; Paris - St. Quentin 1988, 1999, 2005; Melbourne 2002; Prague 2007).

* Corresponding author. Tel.: +420 220 443 808; fax: +420 224 313 200.
E-mail addresses: skvaraf@vscht.cz (F. Škvára), kopecky@fsv.cvut.cz (L. Kopecký), vit.smilauer@fsv.cvut.cz (V. Šmilauer), bittnar@fsv.cvut.cz (Z. Bittnar).
[1] Tel.: +420 224 354 493; fax: +420 224 310 775.

0304-3894/$ – see front matter. Crown Copyright © 2009 Published by Elsevier B.V. All rights reserved.
doi:10.1016/j.jhazmat.2009.02.089

Author's personal copy

Table 1
Average chemical composition of the fly ash.

Component	SiO_2	Al_2O_3	Fe_2O_3	CaO	MgO	Na_2O	K_2O	TiO_2	As_2O_3	V_2O_5	Cr_2O_3	ZnO	PbO	CuO	CdO	Residual C	Total
Weight (%)	51.9	32.8	6.3	2.7	1.1	0.33	2.12	1.89	0.03	0.067	0.29	0.024	0.006	0.011	0.000	0.2	99.57

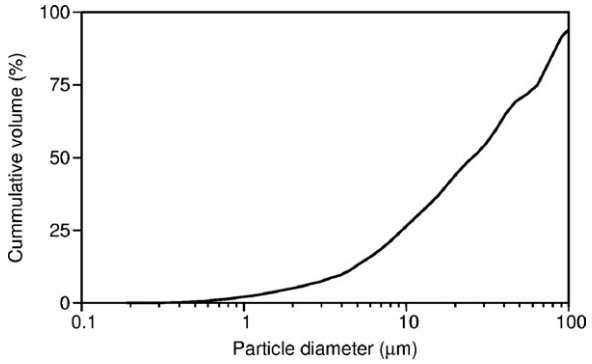

Fig. 1. Particle size distribution of studied RFA.

The maximum of research and investigation of geopolymer materials deals mainly with metakaolines, i.e. thermally activated clays containing a substantial volume of clay minerals such as kaolinite. Several published papers dealt with alkali activation of Ca-rich fly ash [4–6] as opposed to Czech brown coals.

This paper combines both material and technological research of alkali activated waste brown coal fly ash. The results indicate a high compressive strength, excellent durability in chemically aggressive environments plus economic benefits. On the Czech market the current average price of brown fly ash is 500 times lower than that of metakaolin.

2. Source materials and experimental methods

The experimental works utilized brown coal fly ash from Chvaletice thermal electric power plant, Czech Republic, with the Blaine specific surface 210 $m^2\,kg^{-1}$. The average chemical composition of this fly ash is given in Table 1 and particle size distribution in Fig. 1. SiO_2/Al_2O_3 mass ratio is 1.58.

First, fly-ash paste was prepared by mixing with the alkaline activator (NaOH + sodium soluble glass in water solution). The SiO_2/Na_2O ratio (Ms modulus) of alkali activator, i.e. Na-soluble glass (Ms = 2.5), was modified by the addition of NaOH to the target value of Ms = 1.1. Total Na_2O/RFA mass ratio was 7.5%. Water/RFA mass ratio varied from 0.23 up to 0.35 in pastes and mortars, depending on workability issues. The actual compositions of the activators were previously optimized to achieve a high compressive strength, discussed in Section 3.2.1. Mortars were prepared by mixing sand with the paste in the RFA/sand mass ratio of 1:2.5.

The moulds were filled with paste or mortar and put inside the hot-air drier oven in an open atmosphere at 80 °C for 12 h. After 1 day, the moulds were placed in air environment of 40–50% RH until the testing.

The hardened material was tested using a set of instrumental analytical methods to obtain mechanical, mineralogical, physical and chemical complex data at the multilevel. Methods included microcalorimetry (TAM Air), He-pycnometry (Micromeritics AccuPyc 1330), XRD (PANalytical X'Pert PRO Philips), DSC (Setaram DSC 131), TGA (Stanton-Redcroft TG-750), MIP (Autopore III Micromeritics), FTIR (Nicolet 740 Nexus), NMR MAS (^{29}Si, ^{27}Al, ^{23}Na, Bruker

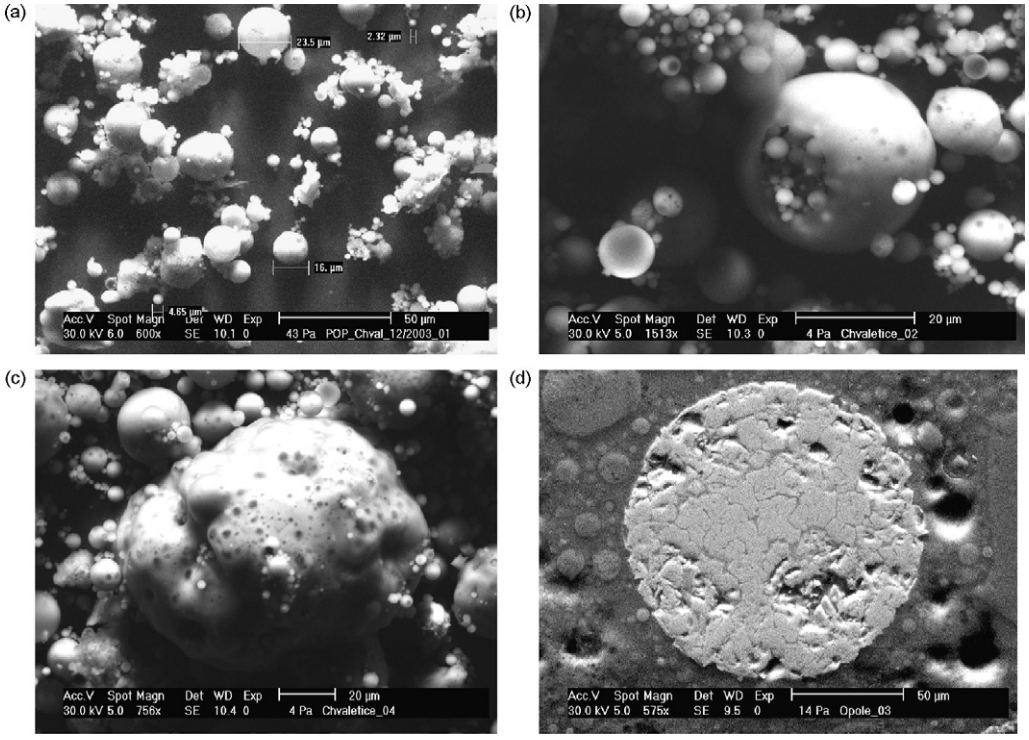

Fig. 2. Characteristic types of particles within fly ash from brown coal: (a) little vitreous particles rich in SiO_2; (b) medium-size conglomerate particles formed by Si–Al vitreous balls, partly enriched in Na–Ca–K–Mg; (c) large heterogeneous particles–formed by conglomerate of vitreous slag highly enriched in Na, K, Ca and Fe; (d) medium-to-small size and compact iron-rich particle formed by polycrystalline aggregate of metallic Fe and Fe(Ti)-oxides (magnetite, hematite, ilmenite).

Author's personal copy

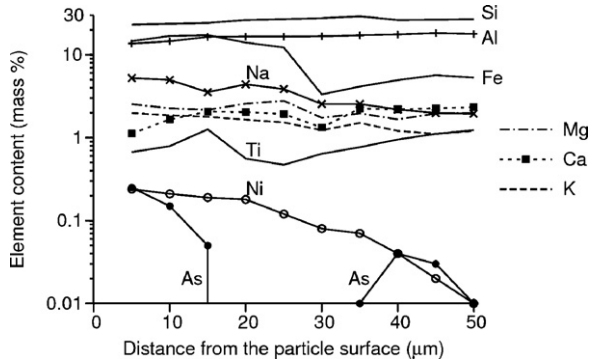

Fig. 3. The variation in chemical (elementary) composition of the medium-size vitreous fly-ash particle taken on profile of the polished section and using EDS analysis.

Avance 500 WB/US), EDS + EBSD (XL 30 ESEM). More detailed study was devoted to RFA (ARL 9400/HP+) using electron microscopy and microanalysis in order to determine the morphology of particles and the chemical composition.

The evolution of the exothermic geo-polymerization reaction was quantified nondestructively by using isothermal calorimetry [6,7]. TAM Air isothermal eight channel calorimeter with a high detectability limit of 4 μW enables the measurement of activation process over weeks. A 4.0 g sample of RFA was activated directly in a modified ampoule with excellent repeatability. The whole measurement took place in temperature-stabilized environment of 20 °C or 60 °C inside the calorimetric unit, therefore the data are not affected even at the onset of activation.

Leachability of geopolymer matrix was determined by using a standardized procedure [8]. Cylindrical samples of 8 mm and 5 mm of height in diameter were fragmented to pieces smaller than 4.0 mm after 90 days of air curing. The fragments were immersed in deionized water in the mass ratio of 1:10 with the first leaching lasting 24 h and consecutive leaching 24 h after. The concentration of ions was determined via AA spectroscopy from 10 ml solution sample.

3. Results and discussion

3.1. Analysis of raw fly ash

Analysis of RFA shows a very heterogeneous material, containing a number of components with different characteristics. RFA originating from the Czech brown coal is typical by its low content of CaO (so-called type F according the ASTM classification) and very high content of As (on average about 300 ppm). Such a high value is also common for eastern Germany due to a localized formation of a sedimentary basin during Tertiary era. Worldwide, the average As content attains values of about 50 ppm [9].

Table 2
Proposed transition from pulverized coal to fly-ash particles after burning.

Original coal mineral composition	Newly formed fly-ash particle
Free quartz	Quartz glass
Clay minerals [without motmorill]	Si–Al slag-like glass, newly formed mullite
Motmorillonite, glauconite, micas	Si–Al [Na, Ca, K, Mg] slag-like glass
Amfiboles, pyroxenes, feldspars	Si–Al [Mg, Fe] glass
Pyrite, marcasite, arsenopyrite	Fe_xO_y [with As, Bi, Hg, Sn . . .]
Hematite, limonite, magnetite	Iron, or Fe_xO_y [rare earth elements]

The initial inspection and separation of basal types of RFA particles was carried out by electron microscopy and analysis. Various types are described in Fig. 2. The formation of RFA particles is operated by a fast burning process in the power plant and depends to a great extent on the primary chemical and mineralogical composition of pulverized coal.

The distribution of elements in a RFA particle is unequal (Fig. 3). Once the carbon has oxidized, the melted substance rich in SiO_2 forms the core of emerging vitreous balls, Fig. 2a), consistent with findings of [10]. Consequently, with a decreasing temperature, the Fe-rich outer rim solidifies around the vitreous ball (Fig. 4). There is a direct implication on the alkaline activation. Alkaline activation is a selective process of alkaline attack on the Ca, Fe and Mg-rich fly-ash particles. These particles are highly porous, enabling easy reaction with the activator.

RFA grains differ in diameter and morphology; both are functions of the chemical (mineral) composition of coal (Table 2). A considerable portion of iron-free particles belongs to hollow glass spheres with high inner porosity (Fig. 2b). The expansion is caused by internal burning of organic microparticles.

EDS analysis revealed dependence between the chemical composition and RFA particle size (Fig. 5). The sequence follows from pure SiO_2 glass, Si–Al oxides, Si–Al [Na, K, Ca] oxides, Si–Al [Mg, Fe] oxides, Fe [Mn, Mg] oxides to iron-rich particles. The finest particles are SiO_2 glass, the very viscose glass melt with high surface tension. Si–Al particles are hollow vitreous balls, sometimes represented by newly formed mullite. Si–Al [Na, K, Mg, Fe, Mn] particles are larger balls of slag-like glass with a highly porous structure. Fe–Mg [Si, Al] are large irregular "pebbles" (slag-like glass particles) filled by a network of bubbles (pores). Fe-rich substances can be easily melted; they coagulate to form large agglomerates. Iron oxides and metallic iron are relatively small balls, caused by the higher melting temperature of iron. The chemical and mineral composition of the incombustible part of coal seems to be the most important factor, followed by the type of technology used in the burning process.

Special attention has been devoted to the distribution of arsenic in RFA. The data generated by EDS analysis both on the profile

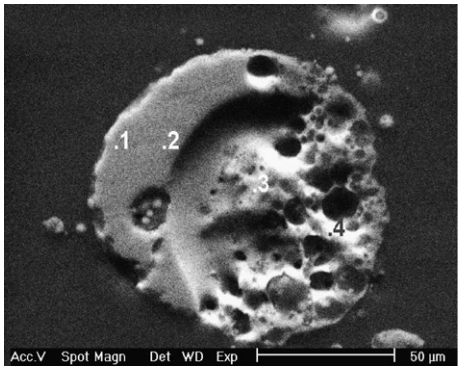

Point	Fe (wt.%)	Si (wt.%)	Al (wt.%)
1	24.1	21.7	13.3
2	24.6	22.9	13.3
3	6.4	32.1	18.3
4	2.9	31.9	19.9

Fig. 4. EDS elementary analysis taken on polished cross section of iron-rich vitreous particle of fly ash. The high iron enrichment in surface parts is evident and results from selected accretion of more easily melted components during solidification at the final stage of burning process.

Author's personal copy

Table 3
Arsenic distribution in regions of different RFA particle types (ppm).

Particle type	Region					
	Surface	Outer	Medium	Inner	Central	Average
SiO_2 glass-compact	400	150	70	0	0	30
Si–Al glass with minor porosity	900	600	150	120	0	120
Si–Al [Na, K, Ca] seedy glass	1700	1600	1100	1000	900	1100
Si–Al [Mg, Fe] slaggy glass	3500	2700	2400	2600	1900	2370
Fe–Mg [Si, Al] slaggy glass	1900	1800	1700	1900	1700	1060
Fe–FeO_x balls with graphite	1000	600	150	90	0	450
Fe [FeO_x] compact little balls	1100	700	250	70	0	190

of individual particle types and in corresponding bulk regions are shown in Table 3. The most important carrier of arsenic seems to be the highly porous slaggy glass, in which the content can attain an average of 2300 ppm. Concerning the spatial distribution of arsenic, the superficial parts of RFA are highly enriched. The phenomenon is caused by the ease of melting and by evaporation of elementary arsenic during the combustible process. The As melting point is 614 °C, while the boiling point is 817 °C. In addition, the arsenic sublimates very easily and condenses on the surface of RFA after cooling.

The ratio between the amorphous and crystalline phases in RFA was determined by XRD Rietveld method using outer standard; 70% (vol.) amorphous phases, 24% (vol.) mullite, 6% (vol.) quartz. The amount of Fe crystalline phases was negligible.

He-pycnometry produced a result of 2.01 g ml^{-1} for skeletal density of RFA. The combination with MIP (intruded into diameters from 3.1 nm to 18 μm) revealed a total porosity of 0.47. The latter contains inter-granular porosity due to improper packing of RFA. High porosity, as observed in electron microscopy, points to hollow objects such ceno- and plerospheres.

3.2. Process of alkali activation

Alkali activation process has been studied and discussed throughout from a chemical and microstructural perspective [11–13], to mention a few. At this point, the role of water during activation process should be stressed especially in the contrast to the system of Portland-based materials. During geopolymerization, water acts as a wetting agent, a carrier of ions (NaOH, soluble water glass), and a donor of H^+ and OH^- ions while dissolving aluminosilicate RFA [14]. A portion of water is returned back in the polycondensation step of gelation, where it pools within the submicron pores [14]. In the presence of Ca ions possibly introduced from, e.g. admixed slag, a portion of capillary water is bound physically and chemically inside C–S–H gels [10]. Not so in fly ash type F where water enters and leaves polycondensation process without much being consumed during geopolymerization. In such a particular case, ultimate capillary porosity is predetermined by the amount of activator and RFA inner porosity (see Section 3.3.3). Cumulative porosities in a similar metakaoline system yielded values between 8% and 20% [14].

Evolution of compressive strength presents an indirect method to monitor microstructure evolution. The case of mortar, with or without the addition of limestone over a period of 4 years is showed in Fig. 6. Here, it is evident that the compressive strength grows continuously, even after several years. The 28-day compressive strength of alkali-activated RFA paste lies between 50 MPa and 80 MPa, whereas in the case of mortar and concrete it is between 35 MPa and 70 MPa. High compressive strength corresponding to high MIP volumes (20–40%) points to an excellent binding capacity of geopolymer. The highest compressive strength for mortar attained 120 MPa while paste achieved 160 MPa, with Ca-rich slag added to both compositions [15].

The interpretation and deeper understanding of alkali activation process at the micro level is explored by means of ESEM. The alkaline activation of fly ash is essentially a selective process caused by significant heterogeneity in the composition of RFA. The ability and kinetics of the reaction depends not only on the chemical and/or mineralogical composition of fly-ash particle but predominantly on the internal structure of the particle, and especially on the specific surface area. The observations show that preferential and rapid activation takes place in the slag-like, large size, Si–Al [Na, K, Mg, Fe, Mn] particles with a rich hollow structure on the micro level, and Fe–Mg [Si, Al] large slaggy RFA particles. The last two particles have never been observed in the products of alkali activated fly-ash geopolymers.

On the other hand, the small vitreous balls, rich in SiO_2 and Al_2O_3 and relatively compact in structure, are remarkable in their homogeneous microstructure and they exhibit a very low degree of alkali attack. A similar effect appears in iron-rich particles composed from the intimate intergrowth of crystals of metallic Fe and Fe oxides, which can be seen in that portion of primary fly-ash material that participates in the alkaline activation process. The latter still remains intact in the heterogeneous matrix. It is necessary to

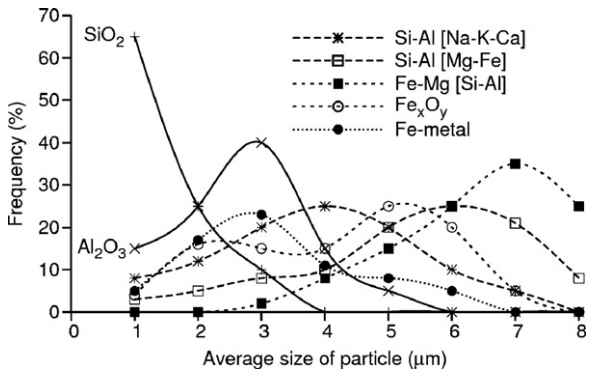

Fig. 5. Relationship between the major chemical composition and particle size of RFA. Heterogeneity in composition is a function of particle size.

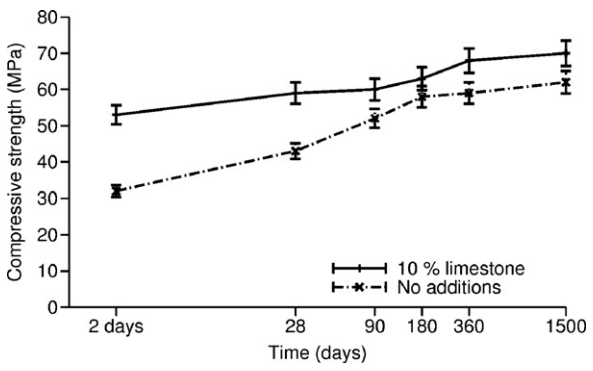

Fig. 6. Compressive strength of geopolymer mortar over a 4-year period, heat curing 12 h at 80 °C.

Author's personal copy

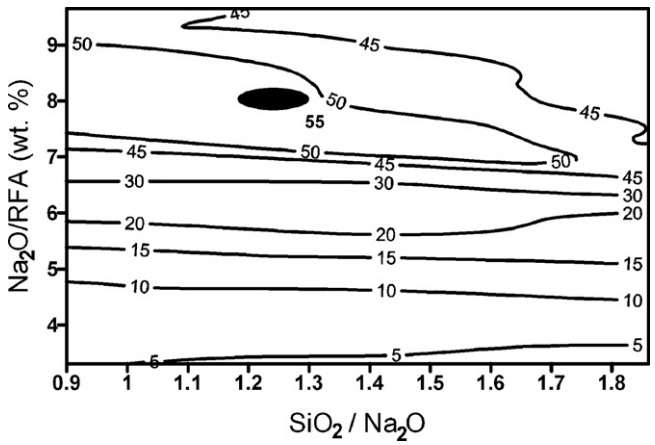

Fig. 7. Optimization of 2-day mortar compressive strength with constant water/RFA = 0.3. Curing at 80 °C for 12 h in open moulds, compressive strength in (MPa).

keep in mind the factor of "weakening" of the "alkali potential" of the residual alkali activators with the progress of activation.

On the molecular level, the process of alkali activation starts with the creation of monomer clusters of SiO_4–AlO_4 tetrahedra from easily soluble parts of RFA particles [16]. The monomer clusters are continuously transformed to amorphous Si–O–Al linear chains and later to an amorphous gel of 2D and 3D network with a different structural configuration. The structural transformation on the molecular level to 3D structures is directly related to an increase of the compressive strength [14]. This is a year-long continuous process (Fig. 6).

The efficiency of activation in terms of dissolved RFA can reach approximately 50% as obtained from ESEM–BSE image analysis. Such a degree of reaction is consistent for 12 h of thermal activation at 85 °C [16]. The analysis proves further that both the metallic (Fe rich) and SiO_2 crystalline parts of RFA are hardly dissoluble in a strong alkaline environment [17,18].

3.2.1. Factors influencing mix design

To achieve the best results both in mechanical properties and durability, we can outline general guidelines suited for the activation of different types of Czech brown fly ash [19,20]. Fly ashes from different locations differ in their reactivity with an alkali activator according to their chemical and mineralogical composition together with the grain size distribution.

Activated Czech RFA of type F needs curing temperature typically between 40 °C and 90 °C, for a period of 4–24 h, although curing at laboratory temperature is possible but results in longer curing times. The formation of C–S–H gel in the C type of RFA richer in CaO, allows attaining reasonable early-age strength under the laboratory temperature.

Studied system of RFA, NaOH solution and Na-water glass has three degrees of freedom for optimization. To explore the domain of compressive strength, former expertise and general guidance were considered [21], yielding fixed water/RFA mass ratio at 0.3, Na_2O/RFA mass ratio between 0.05 and 0.09 and SiO_2/Na_2O ratio between 0.9 and 1.9. RFA/sand mass fraction was 0.5 and the mortar was cured at 80 °C for 12 h in open moulds. Two-day compressive strength in Fig. 7 indicates a dominant role of alkalinity with a minor influence at SiO_2/Na_2O.

Based on this experiment, the mixture proportions mentioned in Section 2 yielded the best compressive strength. A potassium based alkali activator was found less suitable due to lower reaction of RFA [22]. The demand for mixing liquids increases with the narrower particle-size distribution of RFA and also with the content of unburnt residual carbon.

3.2.2. Microcalorimetry monitoring of the alkali activation process

The microcalorimetry experiment was carried out on a simplified system with the exclusion of water glass. NaOH activator of 8 M, 12 M and 16 M was gently injected on 4 g of fly ash inside isothermal environment, while maintaining constant water/RFA mass ratio of 0.4. The focus was given on activator molarity since previous calorimetry results showed a minor influence of activator/fly-ash ratio on a heat flow [7]. Isothermal surrounding temperatures of 20 °C and 60 °C were used throughout the test to estimate the activation energy.

The highest heat flow occurs between 6 min and 12 min after the contact and gradually decreases with subsequent local peaks (Fig. 8) consistent with [6]. The liberated heat, as a measure of reaction degree, is consistent with the model of fly ash alkaline-activation [16], in which the formation of geopolymer gel was determined by the method of selective dissolution.

The activation process resembles the stages of Portland-based systems where the dormant period is left out, followed by accelerator, decelerator and diffusion periods. The degree of reaction after a few minutes is not high; however, it is enough to form an almost impenetrable crust around the fly-ash particle thus preventing the activator from further contact. On the hollow ceno- or plerospheres, the activator dissolves a thin shell while entering the inner space. Such a change is observed as a slump on the macroscale during mixing.

Fig. 8 demonstrates that it is neither the acceleratory nor the decelerator but the diffusion period (above approximately 10 h) that contributes significantly to the progress of activation. An increase of Na_2O in the activator is beneficial only to a certain extent limit; excessive dosage does not improve strength and leads to the presence of free alkali in the sample [6].

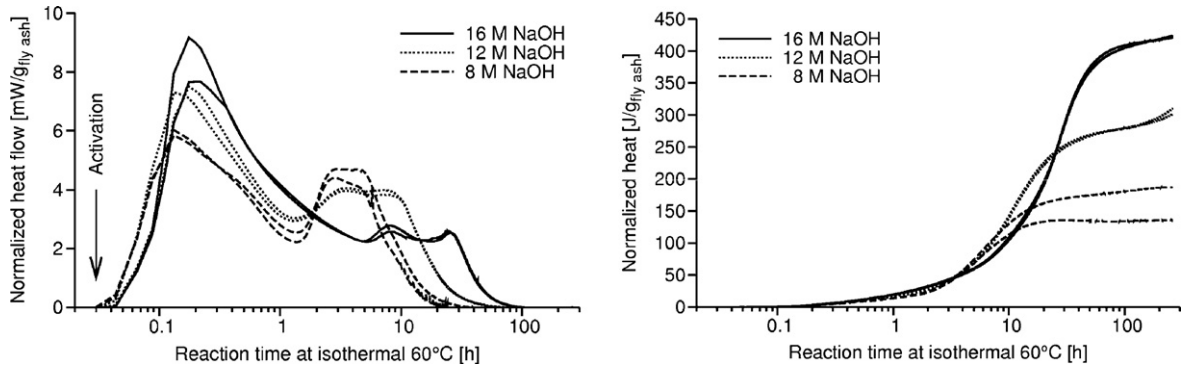

Fig. 8. Normalized heat flow and integrated heat from fly ash activated with three NaOH molar solution, water/RFA = 0.4, isothermal 60 °C.

Author's personal copy

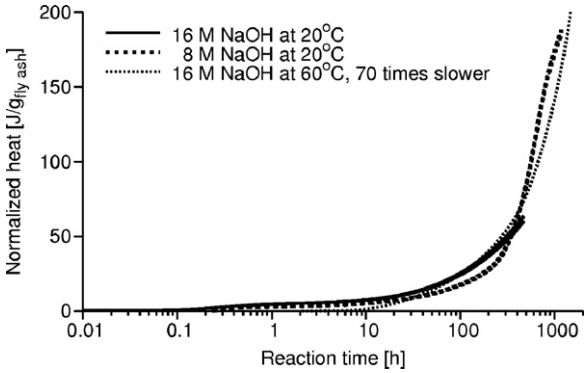

Fig. 9. Heat liberated at isothermal 20 °C using two NaOH activators and the application of maturity principle.

The effect of the curing temperature on identical mixture proportions is demonstrated in Fig. 9. The entire alkali activation at 16 M proceeds approximately 70 times slower at 20 °C than at 60 °C and both kinetics can be related by means of a maturity principle

$$\tau(T_{20}) = \tau(T_{60}) \exp\left[\frac{E_a}{R}\left(\frac{1}{T_{20}} - \frac{1}{T_{60}}\right)\right]$$

where τ represents time mapping at (absolute) temperatures T_{20} and T_{60}, while E_a stands for the activation energy and R for the universal gas constant. For example, activation at 60 °C for 1 day is equivalent to the extent of reaction at 20 °C for 70 days. The kinetics clearly shows that fly-ash activation at the laboratory temperature proceeds considerably slower. The activation energy corresponds to 86.2 kJ/mol, approximately twice as high than in a Portland cement [23].

3.3. Analysis of geopolymers on micro level

3.3.1. Electron microscopy, EDS analysis

Figs. 10 and 11 display the heterogeneous microstructure of geopolymer materials prepared by alkali activation of fly ash. Newly formed geopolymer matrix is highly amorphous. The only crystalline phases originate from residual and sparingly soluble parts of fly ash, namely mullite and quartz. Amorphous phase composition of geopolymer matrix, determined by EDS analysis is represented by Na_2O/SiO_2 ratio in range from 0.1 to 0.3 and Al_2O_3/SiO_2 ratio from 0.25 to 0.35. Total chemical composition of matrix is similar to that of natural zeolite mineral, analcime with the formula $Na_{16}((AlO_2)_{10}(SiO_2)_{26})\cdot 2H_2O$. The representatives of

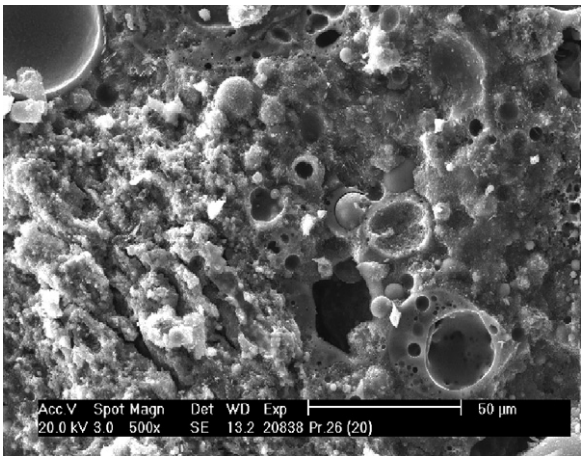

Fig. 10. Typical internal structure of geopolymer paste (ESEM). Note large spherical pores as the relicts of glassy ceno-spheres, rich of silica and alumina.

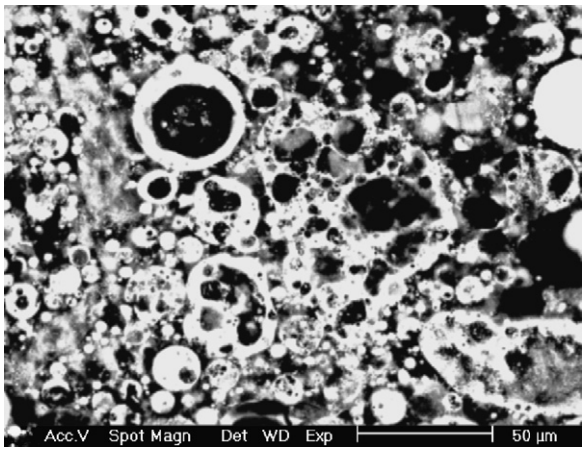

Fig. 11. Polished section of geopolymer paste (BSE).

crystalline phases, aluminosilicates and sodium silicates, were not found in the matrix.

When RFA is blended with slag, cement clinker, or any other calcium bearing material, clinker-like hydrated phases will coexist in the matrix of RFA [10]. Recent experimental results pointed to higher compressive strength when C–S–H coexisted in the matrix. Beyond the reduction in the capillary porosity, we presume that chemical bonding also plays an important role. Ca^{2+} ion can balance the negative charge of two Al atoms in Si–O–Al tetrahedra chains and thus can interconnect only two of them. Conversely, Na^+ ion arising from alkali activators usually balances only one Al atom on one Si–O–Al chain. Sketched models of chemical bonds could explain not only the higher values of compressive strength but also the lower leaching of heavy metals from geopolymer matrix in chemically aggressive environment [19,20,24–28].

3.3.2. Role of water in geopolymer—TGA, DSC

The state of water in geopolymer system resembles that of Portland-based materials. The results from TGA, supported with DSC, in Fig. 12 show that about 65% by mass of all water had evaporated up to 180 °C. The most probable water stage is the "free" and weakly adsorbed, residing in the pores roughly above 5 nm.

Approximately 30% of additional water mass is evaporated at the thermal interval between 180 °C and 600 °C. We presume that this water comes from nano-pores of the geopolymer gel. Total dehydration of geopolymers occurs at around 800 °C.

It should be emphasized that both TGA curves in Fig. 12 are of a smooth nature. No peaks are observed, thus supporting the absence of hydrates in the crystalline form, e.g. $Ca(OH)_2$, $CaCO_3$, or ettringite. Exothermic peaks on DSC curve above 300 °C are probably caused by residual carbon oxidation (Table 1).

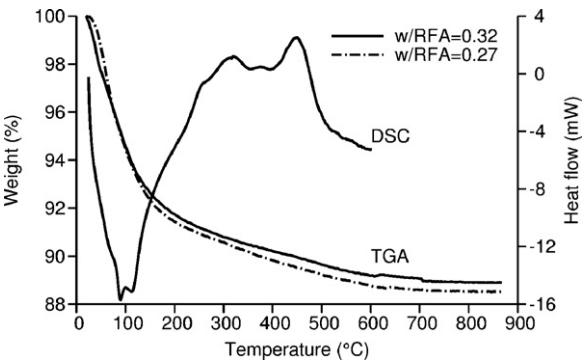

Fig. 12. TGA and DSC results of geopolymer pastes.

Author's personal copy

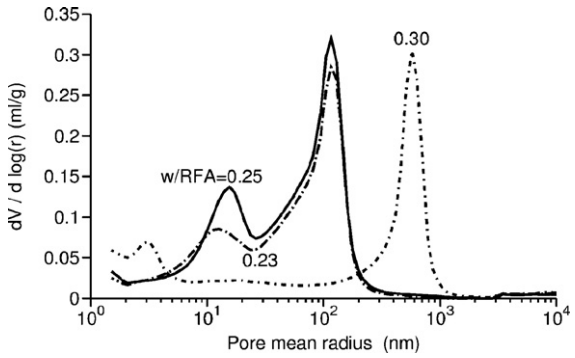

Fig. 13. MIP pore-size distribution in geopolymer pastes with three water/RFA mass ratios.

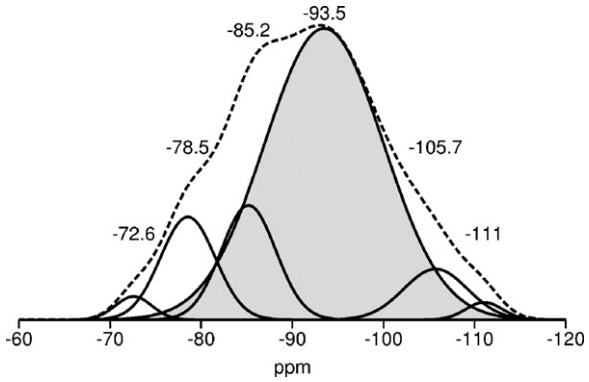

Fig. 15. ^{29}Si NMR MAS deconvoluted spectra of geopolymer paste.

3.3.3. MIP porosity of geopolymer paste

Total porosity of geopolymer paste is influenced substantially by the selection of RFA, which itself contains porosity roughly between 20% and 40%. Since the activation begins immediately after contact with the activator, hollow thin shells are dissolved and the activator can enter the inner space, leading to significant reduction of total volume. Shells rich in iron remain, relatively, intact forever (Figs. 4 and 11) [17,18]. Another source of porosity is represented by the entrapped air introduced during mixing of the highly viscous initial mixture. Regarding Fig. 11, the matrix contains a high portion of pores larger than 1 μm, as identified by image analysis.

Fig. 13 shows MIP pore size distribution in three geopolymer pastes with different water/RFA ratios. Since the same fly ash was used for the preparation, the curve overlap would indicate porosities intrinsic to RFA. However, nothing like that is observed, therefore, the intrinsic RFA porosities must be above the upper range and Fig. 13 displays the results from geopolymer gel filled within the capillary pores. The water/RFA ratio acts as a spacing factor, and the shift to lower pores is systematic while decreasing the ratio. There are no clearly distinguishable regions that are associated with geopolymer gel, probably because these are bellow the 1.5 nm pore radius of MIP.

3.3.4. FTIR and NMR-MAS spectroscopy

The FTIR spectra both of the RFA fly ash and geopolymer paste with a water/RFA ratio = 0.30 reveal a remarkable difference (Fig. 14). The vibration at 1020 cm^{-1} corresponding to Si–O and Al–O in the RFA is shifted below 1000 cm^{-1}. Such a shift is understood as a penetration of Al^{4+} atoms into the original arrangement of Si–O–Si skeletal structure. Similar phenomenon appears in a zeolite structure. The greater the shift of vibration spectrum, the greater the intrusion of Al^{4+} from RFA into the $[SiO_4]^{4-}$ [29,30].

The ^{29}Si NMR MAS spectrum of geopolymer has the shift at −85.2 and −78.5 ppm revealing the coordination of $SiQ^4(3Al)$ and the shift at −93.5 ppm of $SiQ^4(2–3Al)$ coordination (Fig. 15). The shift at −105.7 ppm as a coordination of $SiQ^4(0Al)$ is less represented; thus in fact it reveals the penetration of Al atoms into the $[SiO_4]^{4-}$ network structure. This interpretation is in agreement with other published data [13,31].

The ^{27}Al NMR spectrum of geopolymer displays a dominant peak at 56 ppm corresponding to $AlQ^4(4Si)$ and minor shifts at 84.6 ppm and 1.5 ppm (Fig. 16). The latter corresponds to octahedral aluminium, revealing the remnants of mullite incorporated into the geopolymers matrix from RFA [32,33]. The dominant $AlQ^4(4Si)$ coordination was found in the geopolymers prepared from metakaolin [34,35].

The main shifts of the ^{23}Na NMR MAS spectrum occur at −1.4 ppm, −2.8 ppm and −8.0 ppm, plus weaker shifts at 5.6 ppm and −16.2 ppm (Fig. 17). The same shifts in the interval between −3 ppm and −8 ppm were found in geopolymers prepared from metakaolin [36,37]. These shifts of Na are very similar to that of the structures of hydrated Na-aluminosilicate glasses [36]. Based on [33,36,37] we can deduce that the bond of Na in geopolymer gel (from metakaolin and also fly ash) is in the form of $Na(H_2O)_n^+$, where $n = 2–8$. Na atom reduces the negative charge of the alumina atom in the Si–O–Al structure. The bond of Na in the $Na(H_2O)_n^+$ complex is weaker than the direct bond of Na^+ ion in Al at Si–O–Al chain structure. This model of bonding of the Na atom helps to explain the ease in leaching of sodium out of the geopolymer (regardless of whether prepared from fly ash or metakaolin) and the easy formation of efflorescence on the sample surface. The typical efflorescence on the geopolymer surface (Fig. 18) is composed of hydrates of the type $Na_2CO_3 \cdot nH_2O$, $Na_6(SO_4)(CO_3, SO_4) \cdot nH_2O$.

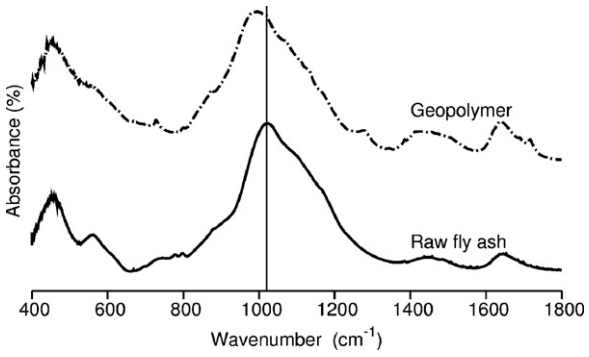

Fig. 14. FTIR spectra of RFA and geopolymer paste.

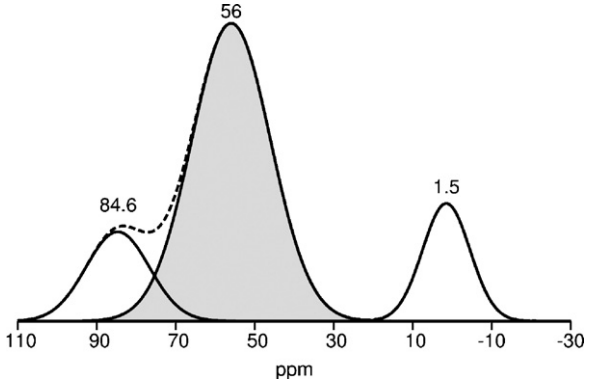

Fig. 16. ^{27}Al NMR MAS deconvoluted spectra of geopolymer paste.

Author's personal copy

Table 4
Leachability of heavy metals from RFA and geopolymer after 24 h (mg/l).

	As	Zn	Cu	Cr	Cd	Pb
Raw fly ash	1.76	0.01	<0.015	<0.04	<0.05	<0.05
Geopolymer	14.3[a], 0.67[b]	0.05	0.05	<0.04	<0.05	<0.05
Limit values[c]	0.05–2.5	5	0.5–1	0.1–1	0.005–0.05	0.1–0.5

[a] 24 h leaching.
[b] Leaching after next 24 h.
[c] Announcement No. 383/2001 of the Ministry of Environment of the Czech Republic (1. and 2. class of leachability).

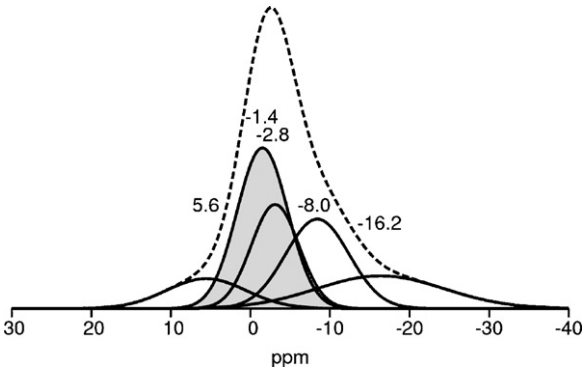

Fig. 17. ^{23}Na NMR MAS deconvoluted spectrum of geopolymer paste.

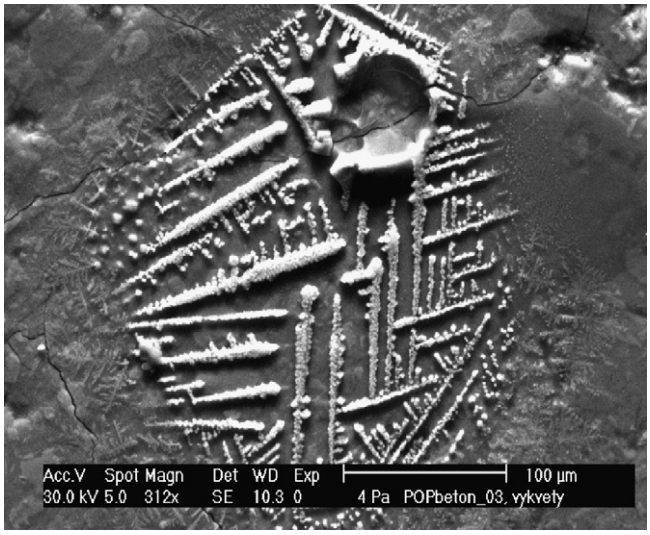

Fig. 18. Typical efflorescence on the geopolymer surface $Na_2CO_3{\cdot}H_2O$, $Na_6(SO_4)(CO_3,SO_4){\cdot}nH_2O$ (natrolit).

There is a good agreement between the above-mentioned results and Barbosa et al. [13]. They express the opinion that the structural coordination of sodium in the form of $Na(H_2O)_n$ is similar to the structure of zeolite and most like analcime. Their model of the molecular structure Si–O–Si of geopolymers made from metakaolin is based on the Na^+ ion surrounded by a ring of H_2O molecules.

Table 5
Kinetics of As leachability from geopolymer (mg/l).

Sampling at	1 h	4 h	6 h	24 h	48 h	72 h
No additive	14.3	14.3	14.4	14.5	14.6	14.7
With 3.5% gypsum	13.2	13.3	13.4	13.5	13.6	13.7

3.4. Leachability of heavy metals from geopolymers

The geopolymer optimized for maximum compressive strength and prepared by the alkali activation of Czech RFA has the ability to immobilize certain heavy metals. Their source is twofold, either originating from RFA itself or from a hazardous material added before a geopolymerization process. Table 4 summarizes leached metals solely from RFA and geopolymer paste with w/RFA = 0.30.

Without the addition of heavy metals, the performance of the geopolymer is in good compliance with the Czech regulations, except for arsenic. As discussed earlier, Czech RFA is rich in As where the principal carriers are pyrites, namely arsenopyrite [9]. The burning process in the power plant transforms the arsenopyrite (and other sulphide minerals) into low saturated oxides rich in iron. Some fraction of As precipitates on the surface of glass spheres. During the alkali activation, As is transformed to the anionic form. These anions are not incorporated into the Si–O–Al chain structure, but only form a weak bond and, as a consequence, they are easily leachable. A similar leaching mechanism applies for Cr^{6+} (but not for Cr^{3+}) which is also present in anionic form [26].

The As leaching occurs predominantly up to 1 h with negligible increase thereafter (Table 5). Even a low addition of gypsum does not help to control the leaching process.

The immobilization of heavy metals, except for As and Cr^{6+}, was previously found very effective in the geopolymer matrix based on RFA [26,38] or slag with metakaoline [39]. The chemical nature of heavy metal compounds also influences their leachability from the matrix [38]. The addition of Ca-rich components such as gypsum or limestone significantly decreases the leachability [38].

The nanostructure M_n $[-(Si–O)_z–Al–O]_n{\cdot}wH_2O$ of geopolymer explains why the cations are generally so well bonded (Table 6). Negatively charged Al anion in Si–O–Al–O– chain is balanced with cation M (Na^+, K^+). Where M stands for diatomic atoms such as

Table 6
Leachability of various metals leached from the geopolymer matrix after 24 h (mg/l).

Added metal (wt%)	Cu added as $CuSO_4{\cdot}H_2O$	Cd added as $CdCO_3$	Cr added as Cr_2O_3	Cr added as $Na_2Cr_2O_7$	Pb as added as PbO
0.5	1.24[a], 0.04[b]	0.32[a], 0.05[b]	0.94[a], 0.04[b]	351	2.73[a], 0.05[b]
1.0	1.19	0.44	1.09	735	7.60
1.5	1.89	0.66	1.97	–	–
2.0	2.77	0.95	2.29	–	–

[a] 24 h leaching.
[b] Leaching after next 24 h.

Author's personal copy

Table 7
Leachability of Zn from geopolymer after 24 h (mg/l).

Zn as metal (wt%)	Zn added as ZnO	Zn added as ZnO + gypsum	Zn added as $ZnSO_4 \cdot 7H_2O$
0.5	2.37[a], 0.07[b]	0.94	5.71
1.0	8.01	1.10	8.41
1.5	16.4	1.89	10.02
2.0	17.3	1.98	12.3

[a] 24 h leaching.
[b] Leaching after next 24 h.

Zn^{2+}, Cu^{2+}, Cd^{2+}, and Cr^{3+}, and an even stronger bond is developed in the case of Cr^{3+}, compensating the charge between two Al atoms simultaneously.

The immobilization of Zn is studied in closer detail since the hydration will cease when the geopolymer is mixed with Portland cement, resulting in a prolonged initial set with very low compressive strength. Table 7 shows excellent Zn immobilization in all three forms.

4. Conclusion

Studied low-calcium brown fly ash is a specific heterogeneous hazardous waste material containing high amount of As. Performed analyses lead to following conclusions

1. Alkali activation is a highly selective exothermic process, attacking preferentially vitreous alumosilicate phases—highly porous slag particles with high internal surface and thus leaving compact glassy balls and iron-rich areas. Internal structure and chemical composition of fly-ash particles are important factors controlling the speed and intensity of ongoing reactions.
2. Synthesized geopolymer exhibits an excellent binding capacity. Compressive strength of mortar exceeds 50 MPa while total porosity remains in the range from 20%–40%. No crystalline phases were detected in the matrix such as C–S–H, C–A–H, $Ca(OH)_2$, aluminosilicates, or sodium silicates. Total dehydration of geopolymer gel occurs around 800 °C. NMR studies did not reveal any principal differences compared to matakaoline-based geopolymer. ^{23}Na NMR MAS resembles the spectrum of hydrated Na-aluminosilicate glasses, hypothesizing that sodium is weakly bound in the form of $Na(H_2O)_n$ rather than Na^+. This would explain why geopolymers are prone to efflorescence in a moisture-gradient environment.
3. Excellent immobilization of diatomic atoms such as Zn^{2+}, Cu^{2+}, Cd^{2+}, and Cr^{3+} was experimentally approved in the geopolymer matrix. As and Cr^{6+} are weakly bonded due to their transformation to the anionic forms. Subsequent As leaching classifies the synthesized material into lower categories, prohibiting its applications for the contact with, e.g. potable water.
4. A geopolymer prepared by alkali activation of fly ash is a new family of inorganic binders originating from waste materials. Mechanical properties are comparable with cementitious materials with superior chemical resistance. Highly favorable environmental impact is evident.

Acknowledgements

This study was part of the research project Czech Science Foundation Grant 103/08/1639 "*Microstructure of inorganic alumosilicate polymers*" and CEZ:MSM 6046137302: "*Preparation and research of functional materials and material technologies using micro- and nanoscopic methods*".

References

[1] A.O. Purdon, The action of alkalies on blast-furnace slag, J. Soc. Chem. Ind. 59 (1940) 191–202.
[2] V.D. Gluchovskij, Gruntosilikaty, Gosstrojizdat, Kiev, 1959.
[3] J. Davidovits, Soft mineralurgy and geopolymers, in: Proceedings of the 1st European Conf. of Soft Mineralurgy "Geopolymer 88", Compiegne, 1988.
[4] M. Criado, A. Fernández-Jiménez, A. Palomo, Alkali activation of fly ash: effect of the SiO_2/Na_2O ratio, Microporous Mesoporous Mater. 106 (2007) 180–191.
[5] A. Fernández-Jiménez, A. Palomo, Composition and microstructure of alkali activated fly ash binder: effect of the activator, Cement Concrete Res. 35 (2005) 1984–1992.
[6] S. Kumar, R. Kumar, T.C. Alex, A. Bandopadhyay, S.P. Mehrotra, Influence of reactivity of fly ash on geopolymerization, Adv. Appl. Ceram. 106 (2007) 120–127.
[7] A. Palomo, M.W. Grutzeck, M.T. Blanco, Alkali-activated fly ashes. A cement for the future, Cement Concrete Res. 29 (1999) 1323–1329.
[8] Announcement No.383/2001 of the Ministry of Environment of the Czech Republic (according to the EU directive).
[9] Ya.E. Yudovich, M.P. Ketris, Arsenic in coal: a review, Intern. J. Coal Geol. 61 (2005) 141–196.
[10] I. Lecomte, C. Henrist, M. Liïegeois, F. Maseri, A. Rulmont, R. Cloots, (Micro)-structural comparison between geopolymers, alkali-activated slag cement and Portland cement, J. Euro. Ceram. Soc. 26 (2006) 3789–3797.
[11] F. Puertas, A. Fernández-Jiménez, Mineralogical and microstructural characterisation of alkali-activated fly ash/slag pastes, Cement Concrete Compos. 25 (2003) 287–292.
[12] S.S. Park, H.Y. Kang, Strength and microscopic characteristics of alkali-activated fly ash-cement, Korean J. Chem. Eng. 23 (2006) 367–373.
[13] V.F.F. Barbosa, K.J.D. Mac Kenzie, C. Thaumaturgo, Synthesis and characterisation of materials based on inorganic polymers of alumina and silica: sodium polysialate polymers, Intern. J. Inorg. Mater. 2 (2000) 309–317.
[14] P. Duxson, J.L. Provis, G.C. Lukey, S.W. Mallicoat, W.M. Kriven, J.S.J. van Deventer, Understanding the relationship between geopolymer composition, microstructure and mechanical properties, Colloids Surf. A: Physicochem. Eng. Aspects 269 (2005) 47–58.
[15] F. Škvára, J. Šlosar, J. Bohuněk, A. Marková, Alkali-activated fly ash geopolymeric materials, in: Proceedings of 11th Intern. Congress Chem. Cement, Cement and Concrete Institute, Durban, 2003.
[16] A. Fernández-Jiménez, A. Palomo, M. Criado, Microstructure development of alkali-activated fly ash cement: a descriptive model, Cement Concrete Res. 35 (2005) 1204–1209.
[17] H. Hamid, D. Leslie, Alkali resistant calcium iron aluminosilicate glass fibers or hollow microsphrees for leaching–resistant cementious compositions, PCT Int. Appl. 2006091929 (2006).
[18] A. Paul, A. Youssefi, Alkaline durability of some silicate glasses containing CaO, FeO and MnO, J. Mater. Sci. 13 (1978) 97–107.
[19] J. Doležal, F. Škvára, L. Kopecký, S. Pavlasová, M. Lucuk, K. Dvořáček, M. Beksa, L. Myšková, R. Šulc, Concrete based on fly ash geopolymers, in: Proceedings of 16th Intern. Baustofftagung IBAUSIL 2006, vol. 1, F.A.Finger Inst. für Baustoffkunde, Weimar, 2006.
[20] F. Škvára, L. Kopecký, J. Němeček, Z. Bittnar, Microstructure of geopolymer materials based on fly ash, Ceramics–Silikáty 50 (2006) 208–215.
[21] A. Fernández-Jiménez, A. Palomo, I. Sobrados, J. Sanz, The role played by the reactive alumina content in the alkaline activation of fly ashes, Microporous Mesoporous Mater. 91 (2006) 111–119.
[22] Ch. Kaps, A. Buchwald, Property controlling influences on the generation of geopolymeric binders based on clay, in: Proceedings of Intern. Conf. Geopolymers, University of Melbourne, Melbourne, 2002.
[23] H. Kada-Benameur, E. Wirquin, B. Duthoit, Determination of apparent activation energy of concrete by isothermal calorimetry, Cement Concrete Res. 30 (2000) 301–305.
[24] F. Škvára, J. Šlosar, I. Jungová, Alkali aktivierte Flugasche–Geopolymere, in: Proceedings of 15th Intern. Baustofftagung Ibausil, F.A.Finger Inst. für Baustoffkunde, Weimar, 2003.
[25] F. Škvára, T. Jílek, L. Kopecký, Geopolymer materials based on fly ash, Ceramics–Silikáty 49 (2005) 195–204.
[26] M. Minaříková, F. Škvára, Fixation of heavy metals in geopolymeric materials based on brown coal fly ash, in: J. Davidovits (Ed.), Proceedings of World Congress Geopolymer, Institut Geopolymére, St. Quentin, 2005.
[27] A. Allahverdi, F. Škvára, Sulfuric acid attack on hardened paste of geopolymer cement, Ceramics-Silikáty 49 (2005) 225–231.
[28] F. Škvára, F. Kaštánek, Geopolymer binder based on fly ash, 2003078349 PCT Int. Appl. (2003).
[29] E. Lippmaa, M. Mägi, A. Samoson, M. Tarmak, G. Engelhardt, Investigation of the structure of zeolites by solid-state high-resolution Si-29 NMR-spectroscopy, J. Am. Chem. Soc. 103 (1981) 1981–4992.
[30] P. Pichat, R. Beaumont, D. Barthomeuf, Infra-red structural study of aluminium-deficient Y zeolites, J. Chem. Soc., Faraday Trans. 1 70 (1974) 1402–1407.
[31] J.G.S. van Jaarsveld, J.S.J. van Deventer, L. Lorenzen, The potential use of geopolymeric materials to immobilise toxic metals, Miner. Eng. 10 (1997) 659–669; J.G.S. van Jaarsveld, J.S.J. van Deventer, L. Lorenzen, The potential use of geopolymeric materials to immobilise toxic metals, Miner. Eng. 12 (1999) 75–86.
[32] H. He, J. Guo, J. Zhu, P. Yuan, ^{29}Si and ^{27}Al MAS NMR Spectra of Mullites from different kaolinites, Phys. Rep. 79 (1981) 331–398.
[33] S. Gomez, M. François, Characterization of mullite in silicoaluminous fly ash by XRD, TEM, and Si MAS NMR, Cement Concrete Res. 30 (2000) 175–181.

Author's personal copy

[34] Chemistry of geopolymeric system, terminology, in: J. Davidovits (Ed.), Proceedings of Geopolymer Intern. Conf. 99, 1999.
[35] R.A. Fletcher, K.J.D. MacKenzie, C.L. Nicholson, S. Shimada, The composition range of aluminosilicate geopolymers, J. Euro. Ceram. Soc. 25 (2005) 1471–1477.
[36] J.A. Tossell, Quantum mechanical calculation of 23Na NMR shieldings in silicates and aluminosilicates, Phys. Chem. Miner. 27 (1999) 70–80.
[37] J.W. Phair, J.S.J. van Deventer, Effect of silicate activator pH on the leaching and material characteristics of waste-based inorganic polymers, Miner. Eng. 14 (2001) 289–304.
[38] M. Minaříková, Leachability of heavy metals from geopolymer on the flyash basis, Ph.D. Thesis, ICT Prague, Faculty of Chemical Technology, 2006.
[39] Z. Yunsheng, S. Wei, C. Qianli, C. Lin, Synthesis and heavy metal immobilization behaviors of slag based geopolymer, J. Hazard. Mater. 143 (2007) 206–213.